Acta Materialia 107 (2016) 38–48

Contents lists available at ScienceDirect

Acta Materialia

journal homepage: www.elsevier.com/locate/actamat

Full length article

In-situ metal matrix composite steels: Effect of alloying and annealing on morphology, structure and mechanical properties of TiB_2 particle containing high modulus steels

R. Aparicio-Fernández, H. Springer*, A. Szczepaniak, H. Zhang, D. Raabe

Max-Planck-Institut für Eisenforschung GmbH, 40237 Düsseldorf, Germany

ARTICLE INFO

Article history:
Received 30 November 2015
Received in revised form
20 January 2016
Accepted 21 January 2016
Available online xxx

Keywords:
Metal-matrix-composites
Steels
Liquid metallurgy
Density
Young's modulus

ABSTRACT

We systematically study the morphology, size and dispersion of TiB_2 particles formed in-situ from Fe–Ti–B based melts, as well as their chemical composition, crystal structure and mechanical properties. The effects of 5 wt.% additions of Cr, Ni, Co, Mo, W, Mn, Al, Si, V, Ta, Nb and Zr, respectively, as well as additional annealing treatments, were investigated in order to derive guidelines for the knowledge based alloy design of steels with an increased stiffness/density ratio and sufficiently high ductility. All alloying elements were found to increase the size of the coarse primary TiB_2 particles, while Co led to the most homogeneous size distribution. The size of the eutectic TiB_2 constituents was decreased by all alloying additions except Ni, while their aspect ratio was little affected. No clear relation between chemical composition, crystal structure and mechanical properties of the particles could be observed. Annealing of the as-cast alloys slightly increased the size of the primary particles, but at the same time strongly spheroidised the eutectics. Additions of Co and Cr appear thus as the best starting point for designing novel in-situ high modulus metal matrix composite steels, while using Mn in concert with thermo-mechanical processing is most suited to adapt the matrix' microstructure and optimise the particle/matrix co-deformation processes.

1. Introduction

Weight reduction represents one of the major challenges for structural materials design. Respective key material properties are not only high strength in order to reduce the wall thickness and hence volume of the part, but also a low density (ρ) and simultaneously a high Young's modulus (E) for improved stiffness. Metal-matrix-composites (MMC's) are of special interest in this light, as they allow blending the property profiles of strong, ductile and tough metallic matrices with stiff and low-density ceramic particles [1,2].

Iron (Fe)-based MMC's, also termed high modulus steels (HMS), are especially attractive, as Fe not only exhibits a similar specific modulus (E/ρ) as f. e. aluminium (about 25 GPa g cm^{-3}), but additionally offers widely scalable mechanical properties due to its multitude of equilibrium and non-equilibrium phase transformations, low production costs and simple recyclability [3,4]. Titanium diboride (TiB_2) has received considerable attention as a respective particle material for HMS design, as it is very effective (E/ρ about 125 GPa g cm^{-3}), can form a strong interface with steel matrices, and, most importantly, can be synthesised in-situ from Fe–Ti–B melts or powder agglomerates in a pseudo-binary eutectic reaction [5–9]. While the liquid metallurgy production of such Fe–TiB_2 in-situ HMS is thus readily possible, the significantly reduced ductility of such composite materials remains a major challenge. A variety of effects was observed to entail brittleness of in-situ metal matrix composite steels: first, the large volume fraction of the ceramic phase, which is required to achieve the desired effect on E/ρ can lead to intrinsically brittle percolation paths through the material. Second, many of the ceramic particles are characterised by sharp-edged shapes which can promote damage initiation. Third, in situ formed ceramic particles in the steel matrix tend to coarsen during the synthesis which facilitates particle fracture upon loading [10–16].

While it was recently shown that the morphology and size of TiB_2 particles can be effectively influenced by tailoring the solidification kinetics [17], another promising pathway to increase the mechanical performance of novel HMS is to utilise alloying

* Corresponding author.
E-mail address: h.springer@mpie.de (H. Springer).

http://dx.doi.org/10.1016/j.actamat.2016.01.048
1359-6454/

additions and thermal/thermo-mechanical processing: As is well established in steel design, alloying elements may be chosen to alter the constitution, phase transformation kinetics, transport coefficients, interface energies, interface cohesion and thus the resultant deformation processes of both, the particles and the metallic matrix [18–20]. In HMS, through some of the effects mentioned above, the alloying elements may also change the particle size and morphology, as f. e. shown in grey cast iron or Al–Si alloys, where the graphite and Si-particles, respectively, are drastically affected by even small additions of e. g. calcium or strontium [21–24]. Furthermore, also the intrinsic properties of the ceramic particles may be affected by possible incorporation of alloying elements within TiB_2. Thermal processing such as annealing treatments (possibly combined with mechanical processing via f. e. rolling) may enhance the associated elemental partitioning of the alloying elements and, most importantly, lead to significant changes not only of the matrix microstructure but also of the particle morphology and heterophase interface properties. Similar effects have been exploited for improving the toughness of high carbon steels through the spheroidisation of hyper-eutectoid cementite lamellae achieved by carefully tuned annealing parameters [3,4]. The combined effects of alloying elements and processing with the aim to alter matrix and particles can thus be systematically utilized to optimise the co-deformation processes occurring when mechanically loading the composite material, thus opening novel pathways for the design of HMS with superior profiles of their physical and mechanical properties.

2. Objective

The objective of this work is to systematically elucidate the effects associated with alloying additions and annealing treatments on the size, morphology, chemical composition, mechanical properties and crystal structure of TiB_2 particles formed in-situ during solidification of Fe–Ti–B based melts. The derived knowledge aims at contributing to the development of guidelines for the mechanism-based alloy design of HMS.

3. Materials and methods

3.1. Alloy production

All alloys presented in this study are of the base composition Fe–10.10 Ti–3.86 B (wt.%). This represents a hypereutectic composition according to the pseudo-binary Fe–TiB_2 phase diagram, corresponding to a TiB_2 fraction of about 20 vol.% [17]. The Ti/B ratio was chosen higher than the exact stoichiometric composition required for TiB_2 in order to suppress the formation of Fe borides [5]. Synthesis was performed by arc-melting 20 g charges of high purity (>99.99%) metals under an argon atmosphere (four times flipping them upside down and remelting for thoroughly homogenisation) on a water cooled copper plate, resulting in a cooling rate at a rate of about 5 K s^{-1} [17]. The following elements were added by 5 wt.% each to the above listed base composition: chromium (Cr), nickel (Ni), cobalt (Co), molybdenum (Mo), tungsten (W), manganese (Mn), aluminium (Al), silicon (Si), vanadium (V), tantalum (Ta), niobium (Nb) and zirconium (Zr). These elements were selected as they represent common alloying additions of steels and can be expected to interact with the TiB_2 formation [3,25,26].

While the emphasis of this study lies on the alloying influence on the resultant microstructures and mechanical properties in the as-cast state, the effects of additional heat treatments was also evaluated for some selected alloys. For this purpose, samples containing Al, Mn, Co, Cr and Mo, respectively, as well as the base alloy, were additionally annealed at 1100 °C for 24 h under argon followed by water quenching to room temperature.

3.2. Characterisation

Cross sections of the button shaped specimen were cut by spark erosion and prepared by grinding and polishing with standard metallographic techniques. The microstructures were investigated by scanning electron microscopy (SEM; Jeol JSM 6490) for imaging and electron backscatter diffraction (EBSD; Jeol JSM-6500F; TSL OIM analysis software 7.2.0). Chemical analysis was performed as qualitative mappings with energy dispersive x-ray spectroscopy (EDX; JSM 6490) in the SEM and quantitatively with an electron probe micro analyzer (EPMA; Jeol JXA-8100, acceleration voltage 15 kV, working distance of 10 mm) with at least 15 measurements each. The crystallographic structural analysis was performed by X-ray diffraction on a Seifert Type ID3003 using Co Kα radiation with a wavelength of 1.78897×10^{-10} m. Rietveld refinement in MAUD version 2.33 software was utilised to calculate the cell parameters of TiB_2, using the harmonic texture model to refine the texture. Transmission electron microscopy (TEM; Jeol-2200FS) was performed on samples of selected alloys prepared with a focused ion beam system (FIB; FEI Helios Nanolab 600i).

Morphology, fraction and size of particles were evaluated by image analysis using the ImageJ software package. We distinguish between particles stemming from primary solidification (coarse, polygonal) and eutectic decomposition (fine, lamellar). The analyses were performed on SEM backscatter electron contrast images at magnifications of 500× for primary and 1000× for eutectic particles, corresponding to areas of 51.3×10^3 and 13.35×10^3 μm^2, respectively.

The mechanical properties, i.e. hardness and reduced Young's modulus (E_r) of primary TiB_2 particles (i.e. those being large enough to be tested) and matrix were probed by nanoindentation using a Hysitron triboindenter and a Berkovich-type indenter at a load of 1000 μN. A minimum of 15 indents were placed in at least three differently oriented particles and matrix grains, respectively. The E_r values were derived from the slope of the load–displacement curve during unloading according to Olivier and Pharr [27].

Liquidus, eutectic and solidus temperatures were calculated by thermodynamic equilibrium calculations using ThermoCalc software and the TCFE7 B–Ti–Fe database with adapted ternary parameters in the liquid phase (supplied by ThermoCalc, Sweden).

All scatter shown for particle sizes and morphology, hardness, E_r and chemical concentrations represent minimum and maximum values.

4. Results

4.1. Morphology and size

Examples of typical characterisation results from the base alloy, i.e. without any alloying additions, are compiled for the as-cast state in Fig. 1. SEM micrographs at different magnifications (Fig. 1a) show the coarse primary TiB_2 particles in square, triangular and hexagonal shapes (top image) and eutectic TiB_2 constituents (bottom image) mostly in form of sharp-edged lamellas as well as in irregular 'flower' or star-like shapes. This deterioration from a strictly regular lamellar morphology as formed under equilibrium conditions can be expected in view of the accelerated solidification rate of the synthesis route chosen here [17]. The measured total particle fraction (primary plus eutectic) of 17.6 vol.% is slightly below the predicted value of 20%. EBSD analysis (Fig. 1b, both maps superimposed with image quality data in grey scale) showed no evidence of intermetallic compounds in the base alloy (phase map

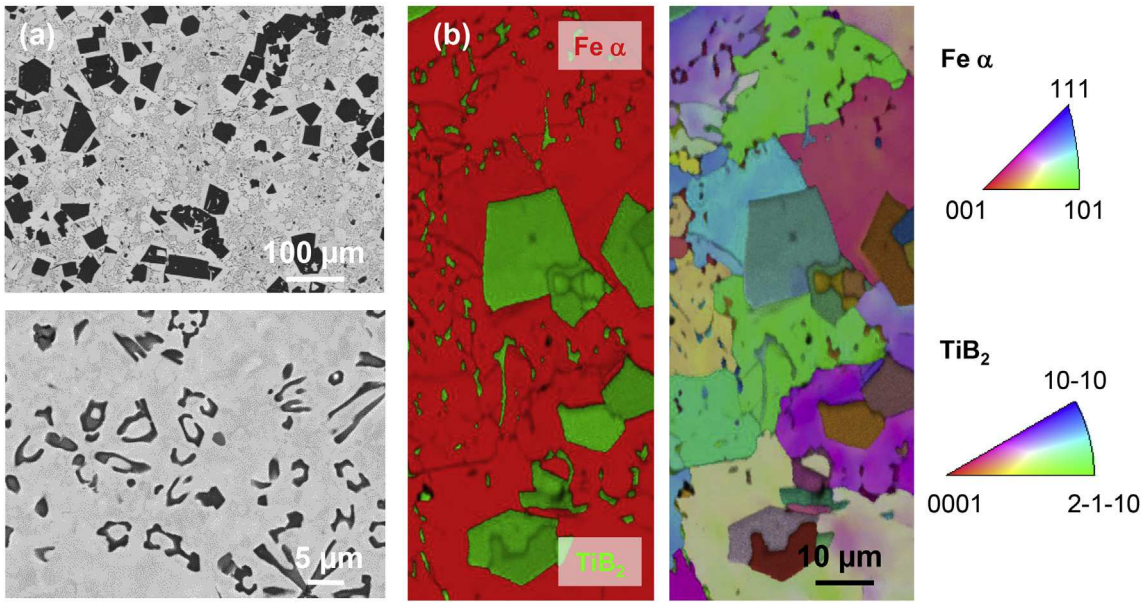

Fig. 1. SEM Characterisation results for the base alloy in the as-cast state. (a) Micrographs of at different magnifications, (b) EBSD phase identification/image quality map (left) and inverse pole figure/image quality maps with corresponding orientations triangles (right).

on the left) and a random orientation distribution of the TiB_2 particles (inverse pole figure map on the right).

As can be seen from the set of low magnification SEM images compiled in Fig. 2 to provide an overview on the different elemental effects, alloying additions leave the shape and morphology of the primary TiB_2 particles almost unaffected in the as-cast state, with the exception of Zr, which leads to the formation of large needle-like structures. The size of the primary particles, however, is profoundly changed by the addition of alloying elements (Fig. 3): All elements were observed to increase the primary particles size, with Cr, Co, Mo, W and Mn causing the smallest coarsening (average size about 50–100 μm^2). Additions of V and especially Zr result in the largest primary particles with average sizes of about 500 μm^2. Co led to the most homogeneous size distribution, i.e. the smallest scatter. Higher magnification images of the eutectic TiB_2 particles (Fig. 4), on the other hand, show much more diverse effects of the alloying additions. The morphology varies now greatly and includes irregular, needle-like, star-shaped as well as rounded particles. Corresponding image analysis (Fig. 5) reveals significant changes concerning size (Fig. 5a) and aspect ratio (Fig. 5b) of the eutectic constituents: All alloying additions except Ni slightly decreased their size. Compared to the primary particles, however, the induced variations are not as pronounced, with average values lying between about 0.5 and 3 μm^2. The aspect ratio of the eutectics particles is less affected by the alloying additions. Cr, Mo, Mn, Al, V and Ta additions slightly decrease the average values, while Ni, Co, Si, Nb and Zr increase them and W shows no significant effect. Ni additions led to the highest and Mo to the smallest scatter in the aspect ratio of the eutectic particles. Alloying with Cr led to the most homogeneous distribution of the eutectic particles across the entire specimen.

The effects of annealing on the microstructure of Fe–TiB_2 based composite steels are compiled in Fig. 6. As exemplified for Co addition in the micrographs compiled in Fig. 6a, two trends can be observed: With the exception of the base alloy, the primary particles coarsened by about 20–50 μm^2, with Mn additions causing the largest relative growth (Fig. 6b). The often inter-connected and sharp-edged eutectic particles inherited from the as-cast state, on the other hand, spheroidised and lost their network-like structure during annealing except for the case of Mo (Fig. 6c). The relative decrease was most pronounced in conjunction with the base alloy and the Co alloyed sample, i.e. after annealing the eutectic particles exhibited an aspect ratio of about 2, close to the ones observed in all of the other alloys investigated here.

4.2. Chemical composition

Qualitative EDX mappings of as-cast samples revealed three different types of effects of the alloying elements: (i) the element is rejected (i.e. not dissolved) by the TiB_2 particles (Ni, Co, Mn, Al, Si), (ii) the element is homogeneously distributed within the particles (Cr, Mo) and (iii) the element is gradually adsorbed into the particles (W, V, Ta, Nb, Zr) creating kinetic transient states and chemically graded particles. These three types of effects, which hold true for both eutectic and primary TiB_2 particles, are quantitatively exemplified in Fig. 7, where the SEM image (top), Ti-concentration (green, middle) and alloying element distribution (red, bottom) are shown for additions of Al (Fig. 7a; rejection), Mo (Fig. 7b; homogeneous dissolution) and W (Fig. 7c; gradual dissolution), respectively. The chemical compositions of both, the primary TiB_2 particles and the solid solution matrix in the as-cast state were quantified by EPMA measurements as shown in Fig. 8. All particles contain between 0.2 and 0.9, within the base alloy up to 2.3 at% Fe. Alloying elements which are dissolved in the particles (homogeneously or gradually) substitute Ti, which is most pronounced for Nb with up to 6.6 at%. All these elements present higher scatter due to gradual adsorption of the element in the particle (Fig. 7). In case of the 'rejected' alloying additions, less than 0.02 at% were detected and the dissolved Fe substitutes B rather than Ti. The amount of Ti and B remains in the stoichiometric range for TiB_2. Those elements rejected by the particles are consequently found in higher concentration in the ferritic matrix (Fig. 8b). This holds true as well for Ti in all alloys due to the chosen over-stoichiometric Ti/B ratio. In case of Nb and Ta, noticeable amounts of B were also found in the matrix (exceeding the solubility of B in α Fe), most probably due to small boride particles in the probed volume. The matrix composition of the Cr-alloyed sample could not be probed due to the homogeneous dispersion of eutectic particles throughout the matrix

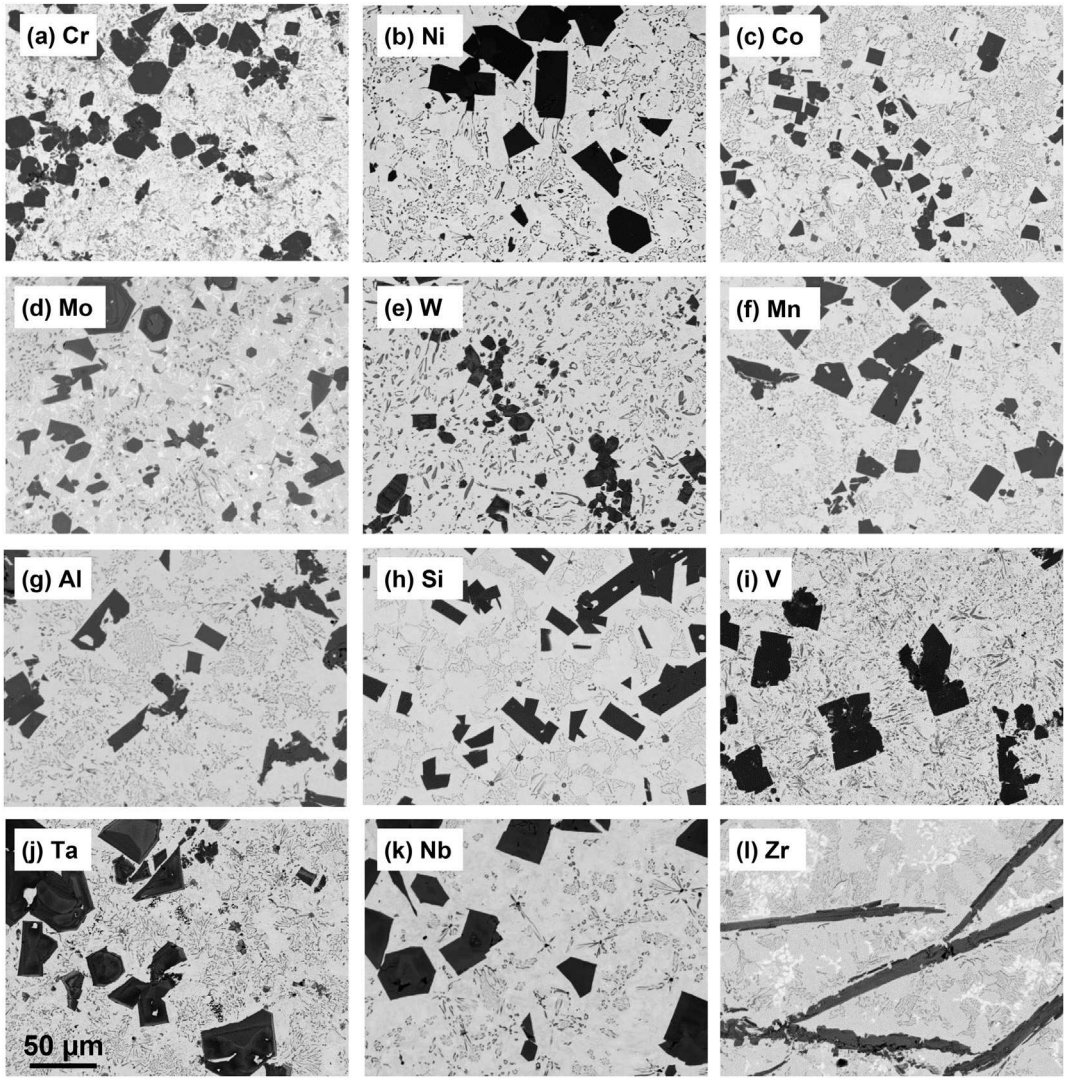

Fig. 2. SEM BEC micrographs of Fe–TiB_2 based composite steels with different alloying additions in the as-cast state.

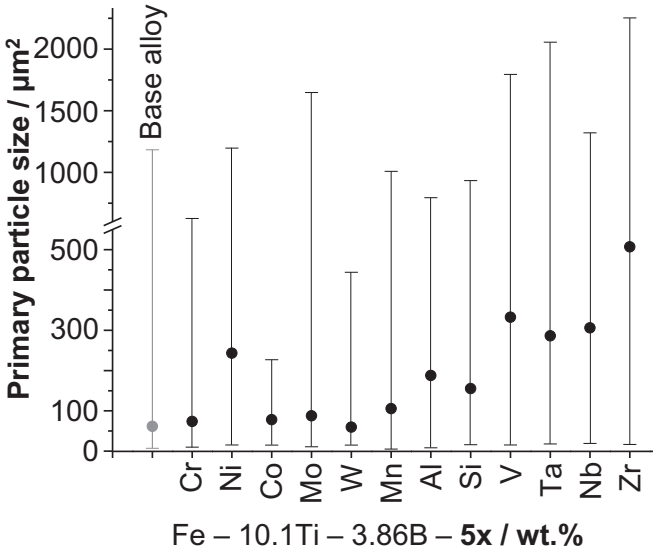

Fig. 3. Size of the primary TiB_2 particles for the different alloying additions in the as-cast state.

(Fig. 4a), affecting the measured values. Analysis of elemental distributions after annealing (not shown here) revealed only minor changes compared to the as-cast state, i.e. a slight evening out of the concentration gradients in case of the gradually dissolved elements.

Unlike for the base alloy without alloying additions (Fig. 1), phases additional to the ferritic matrix and TiB_2 appear to have formed already in the as-cast state, as indicated for example in case of Mo additions by the SEM images (Fig. 2d and Fig. 4d) and EDX mappings (Fig. 7b). While a comprehensive characterisation of all alloys studied here is out of the focus and exceeds the limitations of this work, exemplary results for the Zr-containing alloy are shown in Fig. 9. On the backscatter electron contrast SEM images (Fig. 9a), an additional phase with brighter contrast than the ferritic matrix and TiB_2 can be observed. TEM analysis (Fig. 9b) revealed this phase to be of the Laves type $Fe_2(Zr_xTi_{1-x})$ with Zr concentrations of about 12 at%.

4.3. Crystal structure and mechanical properties

XRD investigations were performed to gain insight into possible changes of the crystal structure of TiB_2 particles due the observed

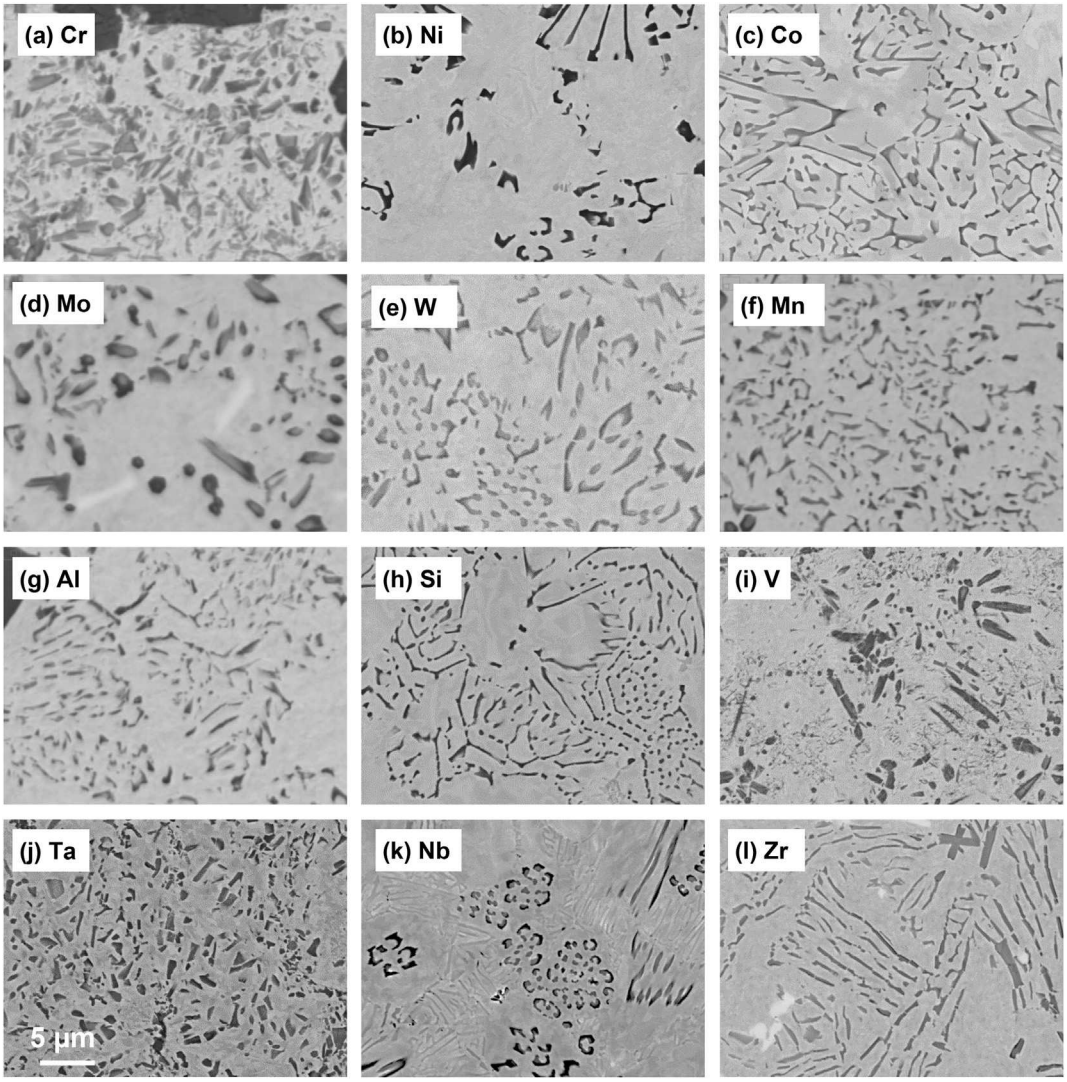

Fig. 4. SEM BEC micrographs of the eutectic areas of Fe–TiB_2 based composite steels with different alloying additions in the as-cast state.

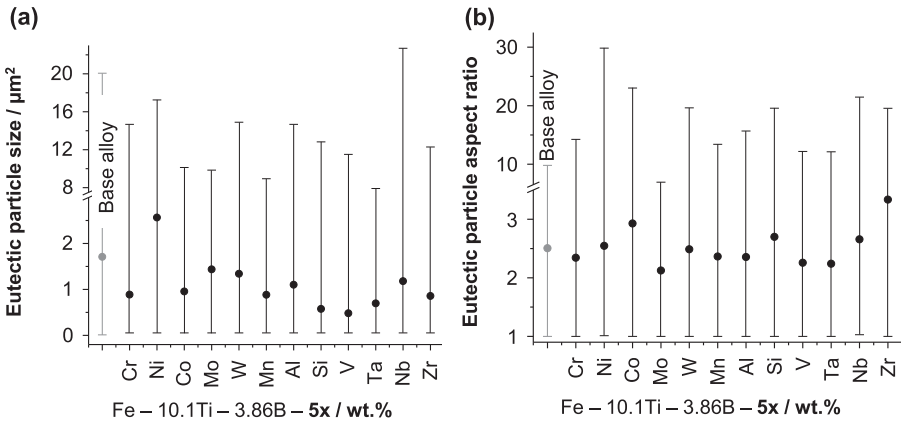

Fig. 5. Eutectic TiB_2 particle size (a) and aspect ratio (b) for different alloying additions in the as-cast state.

alteration in chemical composition induced by the addition of alloying elements. Precise analysis of all alloys of this study, however, was hindered by the aforementioned presence of additional phases, mostly Laves phases and other intermetallic compounds, detected in case of Mo, W, Al, Ta, Nb and Zr additions, as well as by the overlapping of maximum intensity peaks of TiB_2 with α-Fe as the major constituent (matrix). This is visualised in Fig. 10a, where the XRD spectra of alloys with V, Nb and Zr additions are plotted

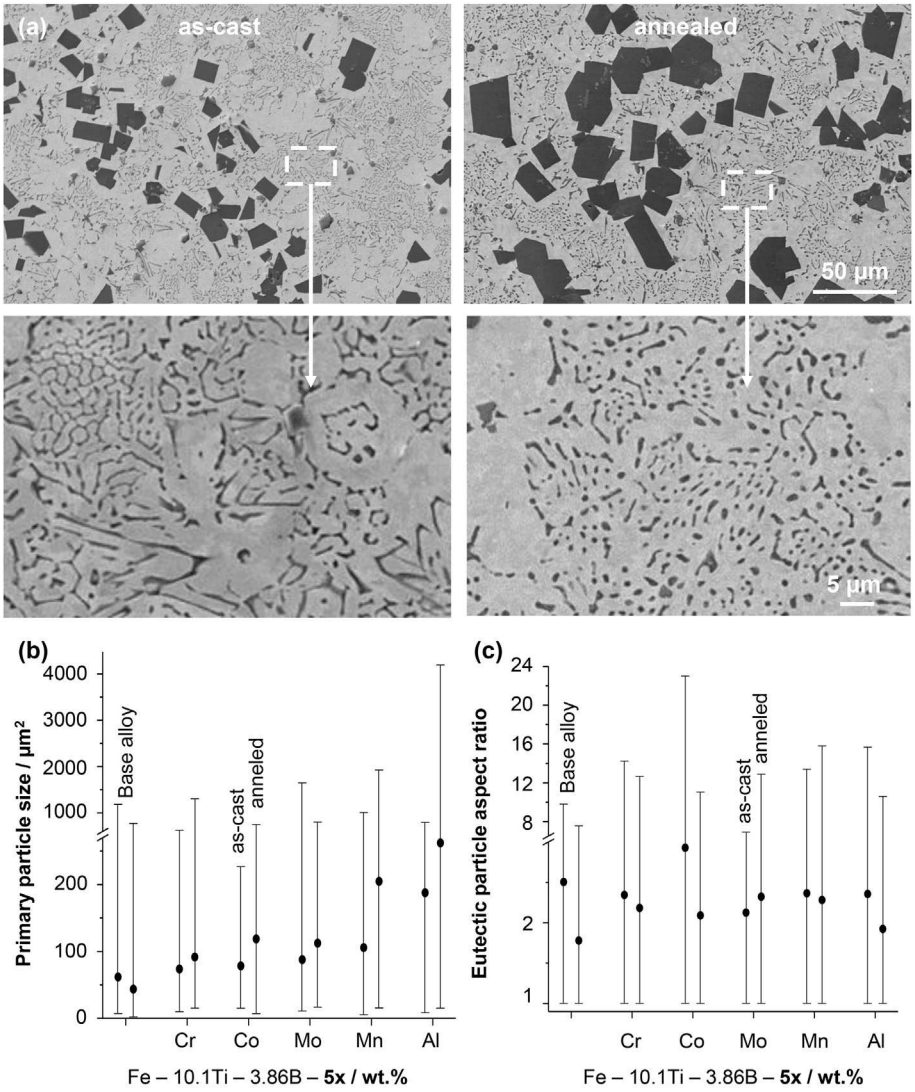

Fig. 6. Effect of annealing on the size and morphology of TiB_2 particles: (a) SEM BEC micrographs of Co additions at different magnifications. Primary particle size (b) and eutectic particle aspect ratio (c) in the as-cast state (left) and after annealing (right), respectively.

together with that obtained from the base alloy (all in the as-cast state). Only in case of these three elements, which were also dissolved to a substantial amount within the TiB_2 (Fig. 8a), noticeable changes in the TiB_2 peak positions could be observed. Rietveld analysis of the shifts of those TiB_2 peaks (2θ = 67.288°, 72.357°, 81.156°, 81.402°, 85.953°, 94.756°, 108.110°, 112.375° and 127.843°) was performed to derive the corresponding lattice parameters a and c as shown in Fig. 10b: While a stays virtually constant, c is slightly decreased by the V addition compared to the value found for the base alloy, and increased by alloying with Zr. No shifts of the α-Fe (matrix) peaks could be observed except in case of Al, which can be attributed to ordering effects [28].

Nanoindentation results for the mechanical properties, i.e. hardness and reduced Young's modulus (E_r) values, are compiled in Fig. 11 for samples in the as-cast state. The TiB_2 particles (Fig. 11a) of the base alloy yield nanohardness values between 15 and 40 GPa (average about 32 GPa) and E_r values ranging from 290 to 440 GPa. The average value of 395 GPa (corresponds to E = 399 GPa at a Poisson ratio of 0.099) is considerably lower than the 515 GPa reported in the literature for polycrystalline TiB_2 [29]. The effect of the alloying-induced changed stoichiometry (Fig. 8) on the Poisson ratio of TiB_2 remains the subject of future research. Together with the relatively high scatter, this demonstrates the general difficulties to accurately probe E_r values by indentation methods, here rendered additionally challenging by the effects of testing relatively small particles being embedded in a much softer and elastically compliant matrix [30]. Nonetheless, relative trends can still be evaluated and described as follows: Al, Si and especially Mn slightly increase, while Co, W and most pronounced Ta decrease the E_r values compared to those of the particles formed in the base alloy. Nanohardness of the particles is slightly increased by all alloying additions except V and Ta, which give lower values. These alloying-induced changes, however, are less pronounced than the E_r alterations, and almost all lie within the scatter of the base alloy data. With respect to the matrix (Fig. 11b), all alloying additions increase its nanohardness, which is expected in view of solid solution strengthening effects and/or the formation of additional phases such as intermetallic compounds. As with the EPMA measurements, the even dispersion of small eutectic particles did not allow to probe the respective matrix of the Cr-alloyed sample. While the E_r values of the matrices show considerable differences between the respective alloying variants, all of them lie within the scatter of

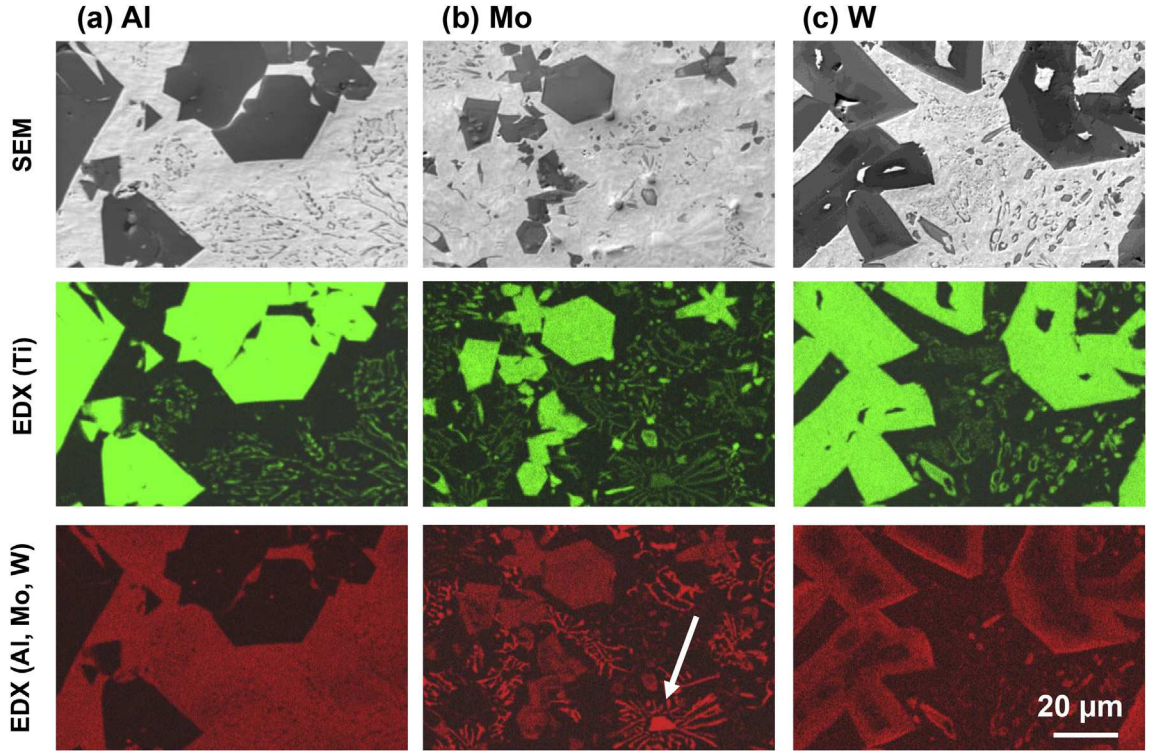

Fig. 7. Qualitative SEM EDX analysis exemplifying the three cases of different alloying elements distribution in the as-cast state: (a) no dissolution in the TiB_2 particles; (b) homogeneous dissolution and (c) gradual dissolution.

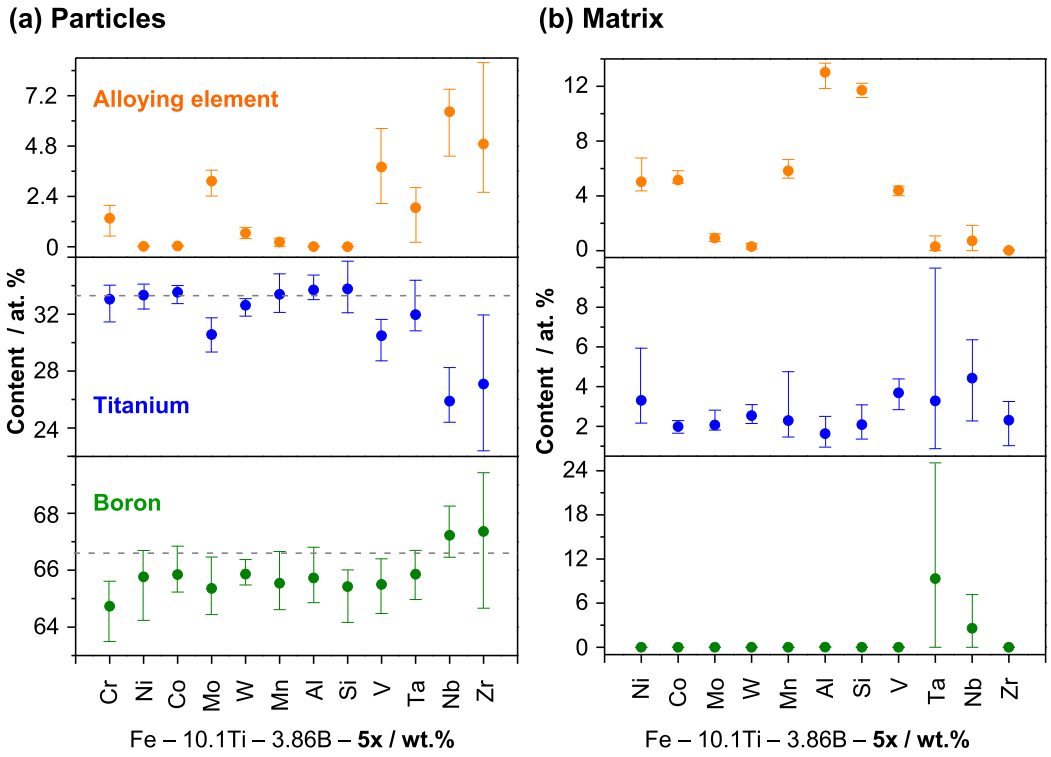

Fig. 8. Quantitative EPMA analysis for the distribution of alloying elements in the as-cast state.

a calibration experiment, performed on a pure Fe sample with more than 5000 indents. Furthermore, the E_r values are most probably additionally affected by the presence of small (eutectic) particles in the probed volume. Hence, the effects of alloying elements on the matrix contribution to the E value of a given composite needs to be evaluated by suitable techniques on bulk materials without particle

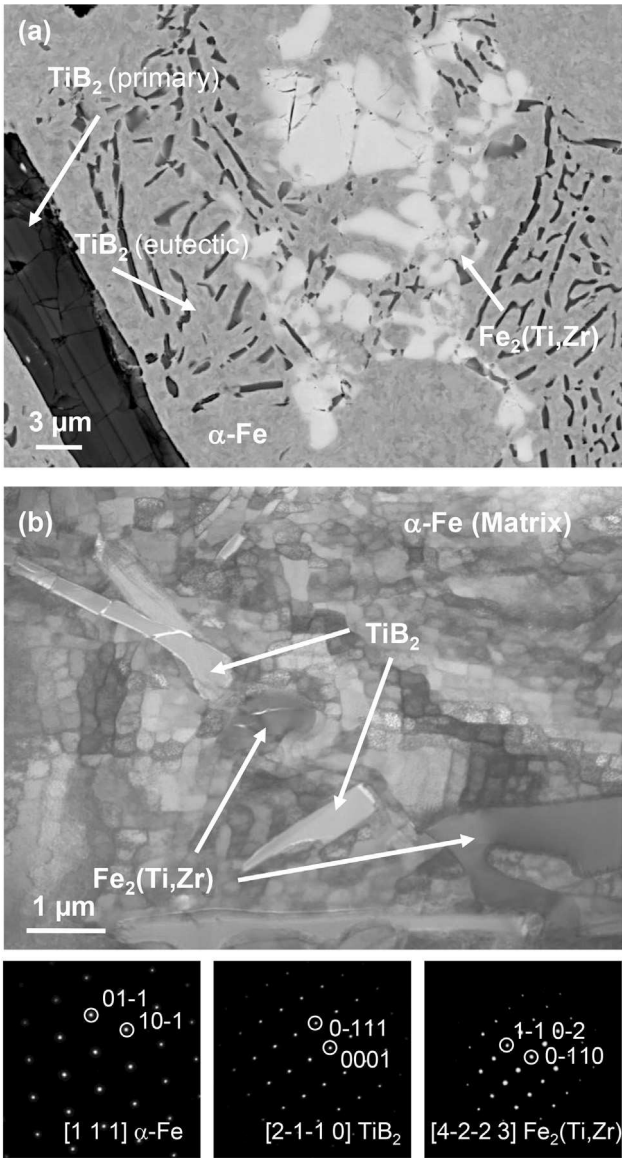

Fig. 9. High resolution microstructure characterisation of the Fe–Ti–B–Zr alloy in the as-cast state. SEM BEC micrograph (a) and corresponding TEM analysis with STEM HAADF micrograph and SAD patterns.

additions [31,32]. The gradual dissolution observed for some alloying elements (Fig. 7) did not lead to a corresponding gradual change in mechanical properties across the TiB_2 particles, the derived values remained in the scatter of measurements in the centre of particles.

5. Discussion

5.1. Relationship between microstructure and mechanical properties

Of all the alloying elements chosen in this study, Cr, Mo, V, Ta, Nb and Zr were dissolved at noticeable concentrations in the TiB_2 particles (partially or gradually; Figs. 7 and 8). This is expected in view of numerous previous findings where Ti and other transition metals of similar position in the periodic system were shown to form diborides over a wide solubility range [25,33,34]. However, only for the case of V, Nb and Zr, which were dissolved to the largest extent (Fig. 8), noticeable changes of the particles' crystal structures could be observed (Fig. 10b). The layered hexagonal structure of TiB_2 exhibits a c/a ratio of 1.067, as the considerably smaller atomic radius of B (80 pm) compared to that of Ti (146 pm) consequently shortens the c-axis compared to the ideal c/a ratio of 1.63 for a hcp unit cell [29,35]. Our EPMA results indicate that the dissolved elements replace Ti (thus changing the stoichiometry of the particles; Fig. 8), and consequently their atomic radius in relation to Ti correlates well with the observed structural changes: While Nb, which has a similar atomic radius as Ti (146 pm), leaves the c-axis virtually unchanged compared to the base alloy, the smaller V (134 pm) elongates and the larger Zr (159 pm) increases the length of the c-axis, respectively. As the a-axis values remained virtually unaffected, these changes directly affect the c/a values (Fig. 10b). However, these structural changes do not translate directly to the observed changes in mechanical properties of the particles (Fig. 11a): The non-dissolved elements, i.e. Ni, Co, Mn, Al and Si, showed stronger effects on the E_r values than the dissolved elements in those cases where structural changes could be measured with sufficiently high precision. It should be noted though that the results of this study are affected by the limitations caused by the given microstructures and respective characterisation techniques. This holds true for the XRD experiments, and especially for the measurements of E_r with nanoindentation techniques. The latter exhibit a large scatter even for bulk Fe (Fig. 11b), as the determination of E_r is highly susceptible to the loading conditions, i.e. increased sensitivity to surface effects with lower loads and increasing 'pile-up'-induced error with larger loads [36]. This highlights the importance of sufficient statistics when probing materials stiffness with indentation methods, as the average value of 208 GPa corresponds well with literature data for Fe [1]. When probing composite materials such as HMS, additional factors such as the presence of small eutectic borides in the probed volume and alloying-induced stiffness of the matrix need to be taken into account. However, while keeping these limitations in mind, and the generally raised complexity of reliably measuring materials stiffness, which—irrespective of the used technique—is often associated with higher scatter than measurements of other material properties [32], the scatter of the values suggests that not too strong effects of alloying additions on the particles and consequently the HMS's physical properties—except of course for respective effects on the matrix [31]—can be expected.

Additional phases beyond the solid solution α-Fe matrix and the precipitate TiB_2 have formed for several alloying additions (Figs. 2, 7 and 9) as can be expected in view of the comparatively high amount of alloying contents and their corresponding binary phase diagrams with Fe. Most common are ordering phenomena (f. e. in case of Al) or Laves phases (f. e. in case of Mo, Nb, Ta or Zr), as confirmed by our results (Fig. 9). A comprehensive study of all phases is complex in view of the large number of alloys from this work, especially in view of the not unambiguously determined Fe–TiB_2 phase diagram (let alone the inclusion of alloying elements). As it thus goes beyond the limitations of this work, which is focused on the effect of alloying elements on the TiB_2 particles as the basis of alloy design; such investigations are subject of future investigations with higher resolution techniques in more detail on specific alloy compositions. The formation of additional Ti-rich phases—either in the as-cast state or during annealing processes—may lower the fraction of TiB_2 particles and consequently lead to the formation of other borides.

5.2. Consequences for alloy design of high modulus steels

A wide range of Fe–TiB_2 based MMC's could be successfully produced by in-situ liquid metallurgy synthesis. The chosen

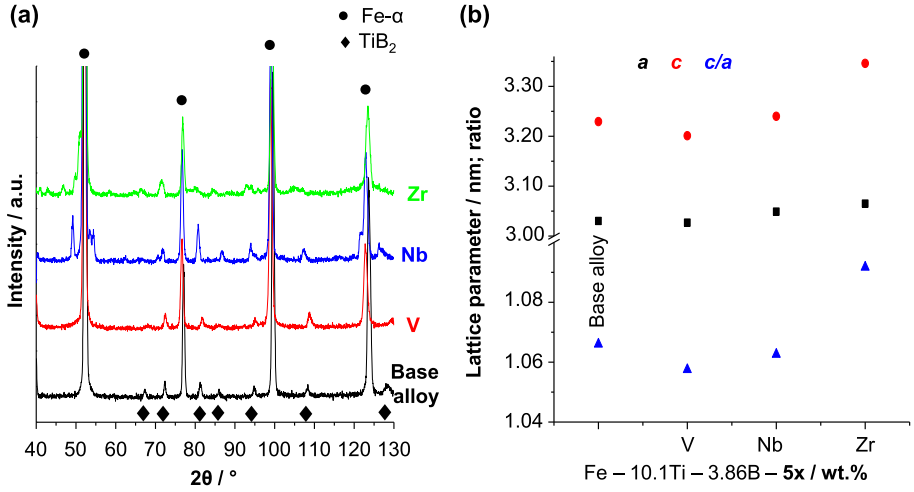

Fig. 10. XRD analysis of the Fe–TiB_2 base alloy base together with spectra for V, Nb and Zr additions: (a) diffractograms, (b) derived lattice parameters and c/a ratio for TiB_2 particles.

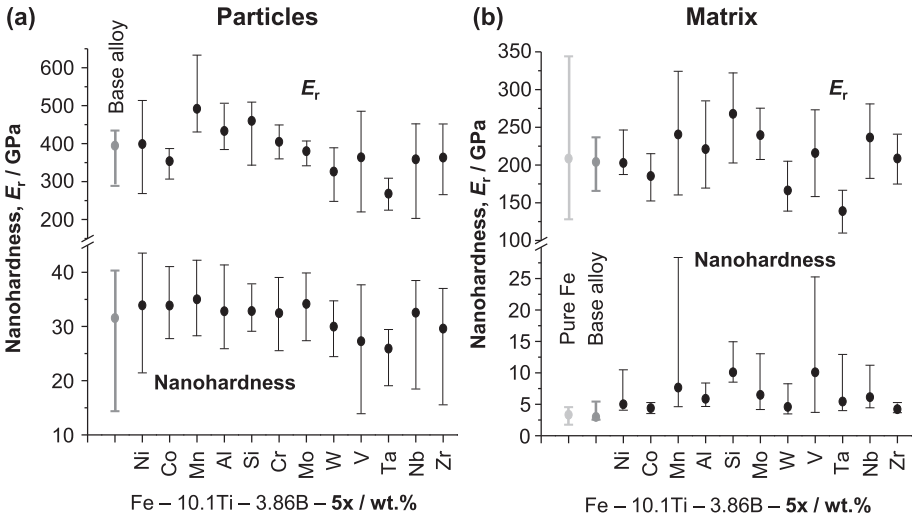

Fig. 11. Nanohardness and reduced Young Modulus values for different alloying additions: (a) TiB_2 particles and (b) Fe-α matrix.

techniques including electric arc melting and rapid solidification generally results in deterioration of the particles' morphology compared to those obtained under equilibrium conditions (especially of the eutectic constituents), but on the other hand represents industrially realistic solidification conditions and, more importantly, ensures a relatively even distribution of the primary particles [17]. The observed clustering of primary particles (Fig. 1) is linked to agglomeration in the melt caused by density-induced floatation [17] and/or sympathetical nucleation [37].

In view of the rather small effects of alloying elements on the properties of the TiB_2 particles (i. e. that most values fall within the scatter of the base alloy data; Fig. 10a), the chemically induced drastic change morphology of the TiB_2 particles (Figs. 2–5)—together with the associated consequences for the matrix properties—can be regarded as the dominant factor for the mechanical properties of the bulk alloy. In grey cast Fe alloys f. e., which may be regarded as in-situ composite materials such as HMS, the spheroidisation of the graphite flakes obtained e.g. by Mg additions leads to superior ductility of the cast materials due to reduced stress concentrations at the graphite/ferrite interfaces and due to the improvement of the volume/surface ratio of the graphite particles [3]. Also, the more spherical the particles are, the better they contribute to the elastic stiffness increase of a composite material [38]. Furthermore, decreasing the size and enhancing the dispersion of the dispersoids or respectively particles is well known to effectively strengthen the bulk composite material, which is exploited for instance in ferritic martensitic dual phase steels [39,40], precipitation-hardened Al-alloys or maraging steels [3,4]. In order to generate HMS with superior mechanical and physical properties, alloy design and processing strategy should thus aim at an even distribution of small and spherical particles in a stiff and ductile metallic matrix.

In the alloy system studied here, the primary TiB_2 particles remained essentially unaffected by alloying, i.e. they prevailed as coarse and sharp-edged squares independent of the chosen alloying element, i.e. as hexagons or more irregular polygons in all cases except for alloys blended with Zr (Fig. 2), where they were shaped as elongated flakes similar to in-situ formed ZrB_2 [41]. This appears reasonable in light of the observed large amounts of dissolved Zr (Fig. 7) and the wide solubility range between ZrB_2 and TiB_2 [42,43]. Co on the other hand most strongly reduced the average size and scatter of the primary particles in the as-cast state (Figs. 2 and 3). Si, V and Ta led to the smallest eutectic particles, Fig. 5a, Cr to their most even, i.e. homogeneous dispersion (Fig. 4a) whereas Cr, Mo,

Mn, Al, V and Ta resulted in the smallest aspect ratio of the eutectic particles in the as-cast state (Fig. 5b). Interestingly, most of these elements were not dissolved within the TiB_2 particles in noticeable amounts (Fig. 8). The reasons for these pronounced alterations of the particles size and morphology thus remain the subject of future work deploying higher resolution characterisation techniques. A possible reason for the changes of the eutectic morphology could be a 'poisoning' of the nucleation sites by intermetallic compounds as it was observed for Al–Si alloys, where ppm additions of Sb, Ca, Na, or Sr lead to intermetallic compounds like Al_2Si_2Sr, which in turn reduce the nucleation frequency of the eutectic Si phase [44–48]. It could be speculated that the size of the temperature range of solidification might be linked to the size of the TiB_2 particles, i.e. that the size of primary and eutectic particles increases with the intervals between liquidus and eutectic temperature and eutectic and solidus temperature, respectively. However, no such trends can be observed when comparing our experimental data (Figs. 2 and 4) with respective thermodynamic calculations (Fig. 12). It should be repeated, though, that the Fe–TiB_2 phase diagram has not been unambiguously determined yet and more experimental data is needed for straightforward predictions of the solidification behaviour of HMS alloys.

From the presented results, utilising additions of Co (for small primary particles) and Cr (for small and well dispersed eutectic particles) seems to be the most promising starting point for future alloy design pathways for in-situ synthesised HMS. Both elements do not appear to deteriorate the E_r values of TiB_2 particles strongly (Fig. 11a) and have the additional effect of increasing E of binary Fe alloys, i.e. here the matrix [31]. Mo and V on the other hand, which - as mentioned above-improve the size and aspect ratio of eutectic particles, readily lead to the formation of intermetallic compounds. The latter compounds are highly undesired as they are also inherently brittle but typically not effective in increasing the E/ρ ratio. Hence, instead of using these comparatively costly elements, exploiting the pronounced spheroidising effects of annealing (Fig. 6) opens thus a much more appealing microstructure design strategy. However, especially when combined with additional deformation such as encountered in hot rolling, possible fracture and delamination of particles (and thus decrease of E and ductility of the bulk steel) due to stresses caused by thermal expansion and shear stresses need to be avoided [49]. Hence the associated processing parameters need to be chosen carefully, also to minimise unwanted coarsening of the primary particles.

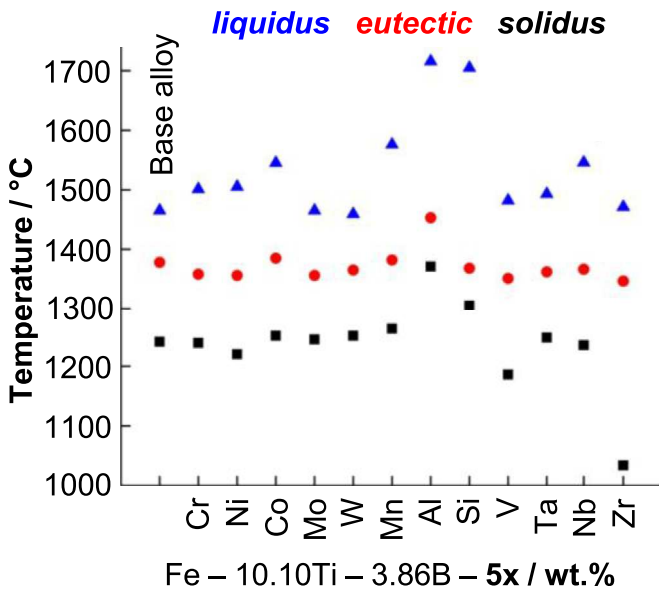

Fig. 12. Liquidus-, eutectic- and solidus-temperatures of Fe–TiB_2 based composite steels with different alloying additions predicted by Thermocalc calculations.

Apart from these changes on the particles, another important aspect for the use of alloying elements is the alteration of the mechanical properties of the matrix. In case of HMS, the strength level, deformation mechanisms, damage tolerance etc. could be thereby adapted to optimise the co-deformation with the hard and stiff particles during mechanical loading. This could be achieved by Mn additions, as this element appears to be relatively neutral on the particle properties and their morphology, leads to the highest E_r values of TiB_2 in our measurements, and can be effectively utilised to achieve stronger and/or more ductile matrices (f. e. austenitic, martensitic or combinations of both) than the ferritic ones which have been the subject of most previous studies [5–9,50,51]. Ni on the other hand is not only more expensive than Mn, but appears also to act detrimental on the particles size and morphology according to our results. Also, the respective physical properties of such altered matrices, namely the lower E of austenitic compared to ferritic Fe, need to be taken into account [32]. The effects of interstitial elements carbon and nitrogen are not as readily described as the substitutional elements used in this study, as they strongly interact with Ti both, during solidification and in the solid state, and thus most likely forms Ti carbides and nitrides in favour of borides. The combined effects of alloying elements, processing parameters and their complex interaction on the resulting microstructures need to be evaluated in the bulk HMS, and may need to be balanced in order to meet the specific goals of the chosen application in terms of both physical and mechanical properties. A promising pathway may be to locally design the HMS microstructure [52] by creating chemical and thereby constitutive gradients around the hard and stiff diboride particles (core-shell-type structures of f. e. ductile austenite surrounding TiB_2), thus minimising the amount of non-ferritic phase fractions and nonetheless improving the overall mechanical performance of the composite material.

6. Summary and conclusions

Here we presented a compositional and microstructure oriented study on the development of in-situ metal matrix composite steels with the aim to provide materials with increased elastic modulus and reduced density. We systematically studied the effects of additions of 5 wt.% of Cr, Ni, Co, Mo, W, Mn, Al, Si, V, Ta, Nb and Zr, respectively, on TiB_2 particles formed in-situ from hyper-eutectic Fe–Ti–B based melts. Morphology, size and dispersion as well as the chemical compositions and crystal structures of the particles, which enable to increase the stiffness/density ratio of steels, where found to be drastically changed by the alloying additions and additional annealing treatments. The following conclusions can be drawn for the knowledge based alloy design of high modulus steels with superior mechanical and physical properties:

(1) All alloying elements led to coarser primary TiB_2 particles compared to the base reference alloy which was synthesized without any additions. Co, however, led to their most even size distribution.
(2) Except for Ni, the eutectic particles for all alloying elements where smaller than in the base alloy. Mo, Mn, Al, V, Ta and Cr, led to smallest aspect ratio in the as-cast state, the latter also to the most homogeneous distribution across the specimen.
(3) Ni, Co, Mn, Al and Si were not noticeably dissolved by the TiB_2 particles, whereas Cr and Mo were homogeneously and W, V, Ta, Nb and Zr gradually distributed within them. No clear relation between chemical composition, crystal structure and mechanical properties of the particles could be

observed. The observation of creating compositional gradients inside the particles, and/or of the surrounding matrix (core-shell-structures) may open future pathways to render the matrix and the particles mechanically more compliant.

(4) Annealing of the as-cast alloys led to slight growth of primary but strong spheroidisation of the eutectic particles, breaking up their network-like structure and decreasing their aspect ratio. Only little effects of annealing on the particles' chemical composition, crystal structure and mechanical properties could be observed.

(5) Based on our results and considering additional effects such as the formation of intermetallic compounds and alloying prices, the most promising starting point for the alloy design of novel HMS seems to be working with additions of Co and Cr for particle modification and using Mn to adapt the matrix' microstructure. Future work will address the possible superposition of the studied effects of alloying elements, the more complex case of the interstitial carbon as well as the investigation of optimisation and exploitation of thermo-(mechanical) processing.

Acknowledgement

H. Bögershausen is gratefully acknowledged for support with the nanoindentation experiments, as are I. Wossack for EPMA and B. Breitbach for XRD analysis.

References

[1] M.F. Ashby, Materials Selection in Mechanical Design, Butterworth-Heinemann, Burlington, MA, USA, 2005.
[2] S.C. Tjong, Z.Y. Ma, Microstructural and mechanical characteristics of in situ metal matrix composites, Mater. Sci. Eng. 29 (2000) 49–113.
[3] H. Berns, W. Theisen, Eisenwerkstoffe: Stahl und Gusseisen, Springer Verlag, Berlin, Heidelberg, 2006.
[4] G. Krauss, Steels: Processing, Structure, and Performance, ASM International, Materials Park, Ohio, USA, 2005.
[5] K. Tanaka, T. Saito, Phase equilibria in TiB_2 reinforced high modulus steel, J. Phase Equilib. 20 (1999) 207–214.
[6] G. Arth, A. Samoilov, Metall matrix verbundwerkstoffe auf eisenbasis, Berg-Hüttenmännische Monatsh. 157 (2012) 306.
[7] Y. Feng, Strengthening of Steels by Ceramic Phases, PhD thesis, RWTH, Aachen, 2013.
[8] A. Antoni-Zdziobek, M. Gospodinova, F. Bonnet, F. Hodaj, Experimental determination of solid liquid equilibria with reactive components: example of the Fe Ti B ternary system, J. Ph. Equilib. Diffus. 35 (2014) 6.
[9] ARCELOR Research group; Patent EP 1 897 963 A1, Bulletin 2008/11 (2008) 20.
[10] Z. Kulikowski, A. Wisbey, T.M.T. Godfrey, P.S. Goodwin, H.M. Flower, Mechanical properties of high performance lightweight steels, Mat. Sci. Tech. 16 (2000) 925–928.
[11] Z. Kulinowski, T.M.T. Godfrey, A. Wisbey, P.S. Goodwin, F. Langlais, H.M. Flower, J.G. Zheng, D.P. Davies, Mechanical and microstructural behaviour of a particulate reinforced steel for structural applications, Mat. Sci. Tech. 16 (2000) 1453.
[12] M.X. Huang, B.B. He, X. Wang, H.L. Yi, Interfacial plasticity of a TiB_2-reinforced steel matrix composite fabricated by eutectic solidification, Scr. Mater. 99 (2015) 13–16.
[13] M. Ziemnicka-Sylwester, L. Gai, S. Miura, Effect of (Ti: B) atomic ratio on mechanical properties of TiB_2–Fe composites “in situ” fabricated via self-propagating high-temperature synthesis, Mater. Des. 69 (2015) 1–11.
[14] L. Gai, M. Ziemnicka-Sylwester, The TiB_2 based Fe matrix composites fabricated using elemental powders in one step process by means of SHS combined with pseudo HIP, Int. J. Refract. Met. Hard Mater. 45 (2014) 141–146.
[15] M. Dammak, M. Gasperini, D. Barbier, Microstructural evolution of iron based metal–matrix composites submitted to simple shear, Mat. Sci. Eng. A 616 (2014) 123–131.
[16] D.H. Bacon, L. Edwards, J.E. Moffatt, M.E. Fitzpatrick, Fatigue and fracture of a 316 stainless steel metal matrix composite reinforced with 25% titanium diboride, Int. J. Fatigue 48 (2013) 39–47.
[17] H. Springer, R. Aparicio-Fernandez, M.J. Duarte, A. Kostka, D. Raabe, Microstructure refinement for high modulus in-situ metal matrix composite steels via controlled solidification of the system Fe–TiB_2, Acta Mater. 96 (2015) 47–56.
[18] L. Cha, S. Lartigue-Korinek, M. Walls, L. Mazerolles, Interface structure and chemistry in a novel steels based composite Fe–TiB_2 obtained by eutectic solidification, Acta Mater. 60 (2012) 6382–6389.
[19] C. Wang, J. Han, J. Miranda Pureza, Y. Chung, Structure and mechanical properties of $Fe_{1-x}Mn_x/TiB_2$ multilayer coatings: possible role of transformation toughening, Surf. Coat. Tech. 237 (2013) 158–163.
[20] I. Sulima, L. Jaworska, P. Wyzga, M. Perek-Nowak, The influence of reinforcing particles on mechanical and tribological properties and microstructure of the steel-TiB_2 composites, J. Achiev. Mater. Manuf. Eng. 48 (2011) 52–57.
[21] S.Z. Lu, A. Hellawell, The mechanism of Si modification in Al–Si alloys: impurity induced twinning, Metall. Trans. A 18 (1987) 1721–1733.
[22] S.D. McDonald, K. Nogita, A.K. Dahle, Eutectic nucleation in Al–Si alloys, Acta Mater. 52 (2004) 4273–4280.
[23] K. Nogita, A. Knuutinen, S.D. McDonald, A.K. Dahle, Mechanisms of eutectic solidification in Al–Si alloys modified with Ba, Ca, Y and Yb, J. Light Met. (2001) 219–228.
[24] A. Pacz, U.S. Patent 1387900, 1921.
[25] K. Takagi, Y. Yamasaki, M. Komai, High strength boride base hard materials, J. Sol. State Chem. 133 (1997) 243.
[26] R. Telle, L.S. Sigl, K. Takagi, in: R. Riedel (Ed.), Boride-based hard materials, Wiley-VCH, Weinheim, 2000, pp. 802–943.
[27] W.C. Oliver, G.M. Pharr, Measurement of hardness and elastic modulus by instrumented indentation: advances in understanding and refinements to methodology, J. Mater. Res. 19 (2004) 3–20.
[28] F. Stein, M. Palm, Re-determination of transition temperatures in the Fe–Al system by differential thermal analysis, Int. J. Mat. Sci. 98 (2007) 7.
[29] G.R. Munro, Material properties of titanium boride, J. Res. Natl. Inst. Stand. Tech. 105 (2000) 709–720.
[30] W. Yan, C.L. Pun, G.P. Simon, Conditions of applying Oliver–Pharr method to the nanoindentation of particles in composites, Compos. Sci. Tech. 72 (2012) 1147–1152.
[31] G.R. Speich, A.J. Schwoeble, W.C. Leslie, Elastic constants of binary Fe base alloys, Metall. Trans. 3 (1972) 2031–2037.
[32] S. Münstermann, W. Bleck, Influences on the elastic modulus of car body steels, Mater. Meas. 47 (2005) 337.
[33] X. Zhang, X. Luo, J. Li, P. Hu, J. Han, Phase stability and mechanical properties of tungsten borides from first principles calculations, Scr. Mater. 62 (2010) 625–628.
[34] H. Kaga, E.M. Heian, Z.A. Munir, Synthesis of hard materials by field activation: the synthesis of solid solutions and composites in the TiB_2 WB_2 CrB_2 system, J. Am. Ceram. Soc. 84 (2001) 2764–2770.
[35] H.Y. Wang, F.Y. Xue, H. Zhao, D.J. Li, First-principles calculation of elastic properties of TiB_2 and ZrB_2, Adv. Mat. Res. 150 (2011) 40–43.
[36] X. Li, B. Bhushan, A review of nanoindentation continuous stiffness measurement technique and its applications, Mater. Charact. 48 (2002) 11–36.
[37] H.I. Aaronson, G. Spanos, R.A. Masamura, R.G. Vardiman, D.W. Moon, E.S.K. Menon, Sympathetic nucleation: an overview, Mat. Sci. Eng. B 32 (1995) 107–123.
[38] J.C. Halpin, J.L. Kardos, The Halpin–Tsai equations: a review, Pol. Eng. Sci. 16 (1976) 5.
[39] M. Calcagnotto, Y. Adachi, D. Ponge, D. Raabe, Deformation and fracture mechanisms in fine-and ultrafine-grained ferrite/martensite dual-phase steels and the effect of aging, Acta Mater. 59 (2011) 658–670.
[40] M. Calcagnotto, D. Ponge, E. Demir, D. Raabe, Effect of grain refinement to 1_ mon strength and toughness of dual-phase steels, Mat. Sci. Eng. A 527 (2010) 2738–2746.
[41] A.K. Shurin, V.E. Panarin, Phase equilibria and structure of alloys Fe-ZrB_2, Fe-TiB_2 and Fe-HfB_2, Izv. Akad. Nauk. SSSR Met. 5 (1974) 235–239.
[42] S. Chakraborty, D. Debnath, A.R. Mallick, P.K. Das, Mechanical and thermal properties of hot pressed ZrB_2 system with TiB_2, Int. J. Refract. Met. Hard Mater. 46 (2014) 35–42.
[43] X. Zhang, P. Hu, S. Meng, J. Han, B. Wang, Microstructure and mechanical properties of TiB_2 Cu Ni interpenetrating phase composites, Eng. Mater. 312 (2006) 287–292.
[44] A.K. Dahle, K. Nogita, J.W. Zindel, S.D. McDonald, L.M. Hogan, Eutectic nucleation and growth in hypoeutectic Al–Si alloys at different strontium levels, Metall. Mater. Trans. A 32 (2001) 949–960.
[45] A.K. Dahle, K. Nogita, S.D. McDonald, C. Dennis, L. Lu, Eutectic modification and microstructure development in Al–Si alloys, Mat. Sci. Eng. A 413 (2005) 243–248.
[46] P. Srirangam, S. Chattopadhyay, A. Bhattacharya, S. Nag, J. Kaduk, S. Shankar, R. Banerjee, T. Shibata, Probing the local atomic structure of Sr-modified Al–Si alloys, Acta Mater. 65 (2014) 185–193.
[47] M. Zarif, B. McKay, P. Schumacher, Study of heterogeneous nucleation of eutectic Si in high-purity Al–Si alloys with Sr addition, Metall. Mater. Trans. A 42A (2011) 1684–1691.
[48] R. Aparicio, G. Barrera, G. Trapaga, M. Ramirez-Argaez, C. Gonzalez-Rivera, Solidification kinetics of a near eutectic Al–Si alloy unmodified and modified with Sr, Met. Mater. Int. 19 (2013) 707–715.
[49] R. Rana, C. Liu, High modulus steels, Can. Met. Quart. 53 (2014) 300.
[50] N. Yang, I. Sinclair, Fatigue crack growth in a particulate TiB_2 reinforced powder metallurgy Fe based composite, Metall. Mater. Trans. A 34 (2003) 2017.
[51] F. Ayari, E. Bayraktar, Fretting wear damage I numerical study of composite steel sheets reinforced with TiB_2, Arch. Mat. Sci. Eng. 50 (2011) 48.
[52] M. Belde, H. Springer, G. Inden, D. Raabe, Multiphase microstructures via confined precipitation and dissolution of vessel phases Example of austenite in martensitic steel, Acta Mater. 86 (2015) 1–14.